Available online at www.sciencedirect.com
SCIENCE DIRECT®
Continental Shelf Research 24 (2004) 375–392
CONTINENTAL SHELF RESEARCH
www.elsevier.com/locate/csr

Turbulence spectra and local similarity scaling in a strongly stratified oceanic bottom boundary layer

Ren-Chieh Lien*, Thomas B. Sanford

Applied Physics Laboratory, University of Washington, 1013 NE 40th Street, Seattle, WA 98105, USA

Received 8 November 2002; received in revised form 30 June 2003; accepted 14 October 2003

Abstract

In the turbulence inertial subrange, wavenumber spectra of vertical velocity and streamwise velocity in a strongly stratified oceanic bottom boundary layer agree with the local similarity scaling laws found previously in the stable atmospheric boundary layer. At scales greater than the turbulence inertial subrange, oceanic velocity spectra exceed the universal spectra. This additional energy at large scales could be due either to internal waves, inappropriate estimates of turbulence parameters, or non-stationarity of the data. Providing that the energy containing eddies in the stratified boundary layer have a scale close to the Ozmidov scale, $\varepsilon^{1/2}N^{-3/2}$, where ε is the turbulence kinetic energy dissipation rate and N is the buoyancy frequency, the universal model spectrum leads to a turbulent scaling $\varepsilon = \beta N\sigma_w^2$, where β is a dimensionless constant 0.6–1.5 and σ_w^2 is the vertical velocity variance. This scaling law of ε has been found in free shear flows in the ocean and atmosphere. The turbulence Reynolds stress is related to the vertical velocity variance as $-\langle u'w' \rangle = 1/4\sigma_w^2$. The strong stratification in the observed tidal bottom boundary layer is maintained by the advective density gradient. Results reported here include the effects of horizontal advection.

Keywords: Turbulence; Similarity scaling; Bottom boundary layer; Internal waves

1. Introduction

Within turbulent boundary layers, turbulent fluxes are important dynamically. In numerical models, turbulent fluxes need to be parameterized with numerical schemes based on empirical formulas or theoretical arguments and, sometimes, with delicate tuning. Empirical formulas of turbulent fluxes are determined by combining field observations, laboratory experiments, and theory.

It was recognized in the 1950s that scaling laws describe atmospheric boundary layers. The famous Monin–Obukhov (MO) similarity-scaling theory was first proposed (Obukhov, 1971) and then confirmed with measurements (Monin and Obukhov, 1954). The MO similarity theory suggests that turbulence and mean properties within the surface boundary layer are determined by surface stress, surface buoyancy flux, and the distance from the boundary. Based on MO scaling, Businger et al. (1971) derived empirical formulas for the temperature and wind gradients under unstable, neutral, and stable conditions using simultaneous measurements of surface fluxes and

*Corresponding author.
E-mail address: lien@apl.washington.edu (R.-C. Lien).

0278-4343/$ - see front matter © 2003 Elsevier Ltd. All rights reserved.
doi:10.1016/j.csr.2003.10.007

profiles of temperature and wind. These empirical formulas have been used to justify the parameterization schemes in numerical models (e.g., Mellor and Yamada, 1982).

Mahrt (1999) provided an ideal view of the stable turbulent boundary layer which consists of the roughness sublayer, surface layer, local-similarity layer, and z-less layer (Fig. 1). Heights of these layers are modified by the background stability. Above the surface layer, the MO similarity scaling fails because turbulent fluxes generated by other processes, e.g., breaking internal waves and local shear instability, may be equally important as surface fluxes. Nieuwstadt (1984) proposed a local MO similarity scaling in which mean and turbulent properties are scaled by the local turbulent fluxes following the same MO formulas. The z-less layer is an extension of the local scaling layer for $z \gg$ the local Monin–Obukhov length scale L. Wyngaard and Kosovic (1994) argued that turbulence properties in the stable boundary layer are variable due to unsteadiness, baroclinicity, terrain slope, and breaking internal gravity waves. Generally it is uncertain whether the local similarity scaling should apply in the intermediate to the strongly stratified turbulent boundary layer.

The oceanic turbulent boundary layer is not as well studied as the atmospheric counterpart because of the difficulty of oceanic measurements. The oceanic surface boundary layer is similar to the atmospheric surface boundary layer, but not identical, because surface gravity waves and coupled processes between turbulence and waves, such as Langmuir circulation, are often present (Fig. 1). Turbulence generated by breaking surface gravity waves (e.g., Drennan et al., 1996; Terray et al., 1996; Gemmrich and Farmer, 1999) and associated with Langmuir circulation (McWilliams et al., 1997) is clearly not accounted for in the MO similarity scaling (Anis and Moum, 1995).

Sanford and Lien (1999) and Lien and Sanford (2000) confirmed the MO similarity scaling in an unstratified oceanic bottom boundary layer. In stratified condition, however, the surface buoyancy flux is important in the atmospheric surface

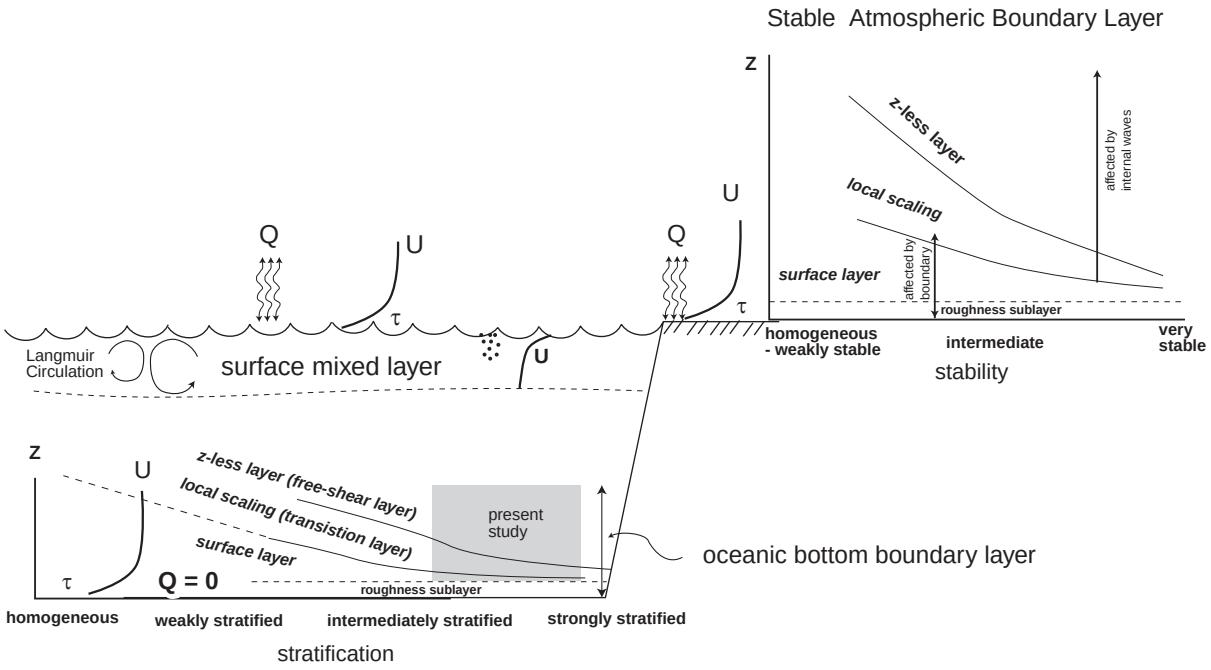

Fig. 1. Sketch of flow regimes in stable atmospheric boundary layer (after Mahrt, 1999) and oceanic bottom boundary layer. Q represents the interfacial buoyancy flux and τ is the interfacial stress. U represents a time mean velocity profile.

boundary layer and is the primary parameter of the MO similarity scaling, but the oceanic bottom boundary layer lacks the buoyancy flux at the sea bed (Fig. 1). Obviously, the MO similarity scaling breaks down in the stable oceanic bottom boundary layer. One may suspect the local similarity scaling (Nieuwstadt, 1984) to be applicable above the surface layer of the oceanic bottom boundary layer. To our knowledge, there has been no documented evidence of the local similarity scaling found in the stratified oceanic bottom boundary layer.

The primary objectives here are to examine turbulence velocity spectral properties and similarity scaling laws in a strongly stratified oceanic bottom boundary layer using measurements taken in a tidal channel. The following section describes experiments and measurements. Section 3 reviews the model spectrum obtained in the stable atmospheric boundary layer and velocity spectra observed in the stratified oceanic boundary layer. Similarity scalings of the turbulence kinetic energy dissipation rate and the momentum flux are discussed in Section 4. In Section 5, the difficulty of separating internal waves and turbulence in a stratified bottom boundary layer is discussed.

2. Experiments and measurements

Data described in this paper were taken in the turbulent boundary layer of a tidal channel, Pickering Passage, WA, during spring ebb tides (Fig. 2). The average water depth at the experiment site was ~22.5 m; it decreased from 25 to 20 m during the ebb tide. A detailed description of the experiment site and bathymetry are presented in Sanford and Lien (1999). Five experiments were conducted between 1993 and 1998 denoted as PP1–5. All five experiments were taken upstream of a ~4-m high ridge, except a 1.5-h segment of measurements in PP4 taken downstream of the ridge and excluded from this analysis. Measurements were taken by sensors mounted on the electro-magnetic vorticity meter (EMVM) towed-body operated from the anchored R/V *Miller* of APL-UW (Fig. 3). The EMVM towed-body was either profiled vertically through the water column or held at fixed depths. The primary sensor mounted on the towed-body was the vorticity meter (VM), which measured turbulence velocity and vorticity using the principle of motional induction. Several other sensors were mounted on the EMVM towed-body: a CTD, a shear probe

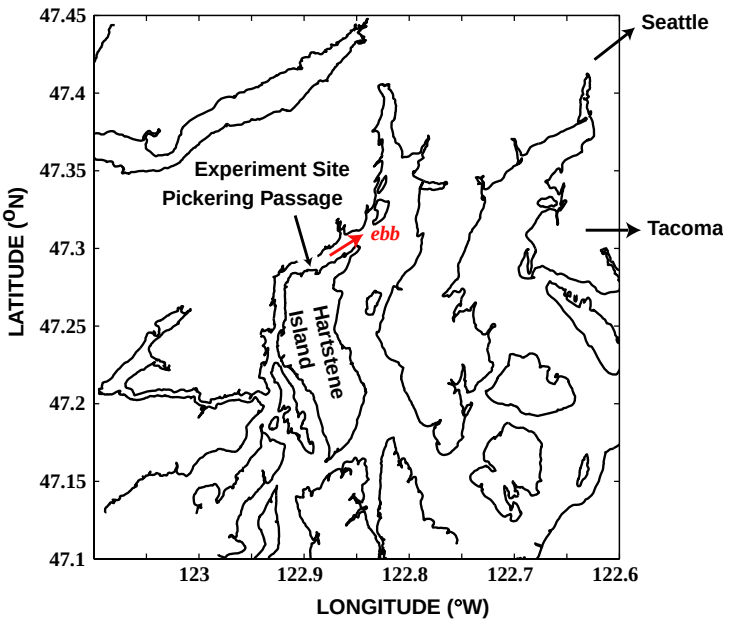

Fig. 2. The experiment site, Pickering Passage of Washington. The arrow shows the direction of the ebb tidal current.

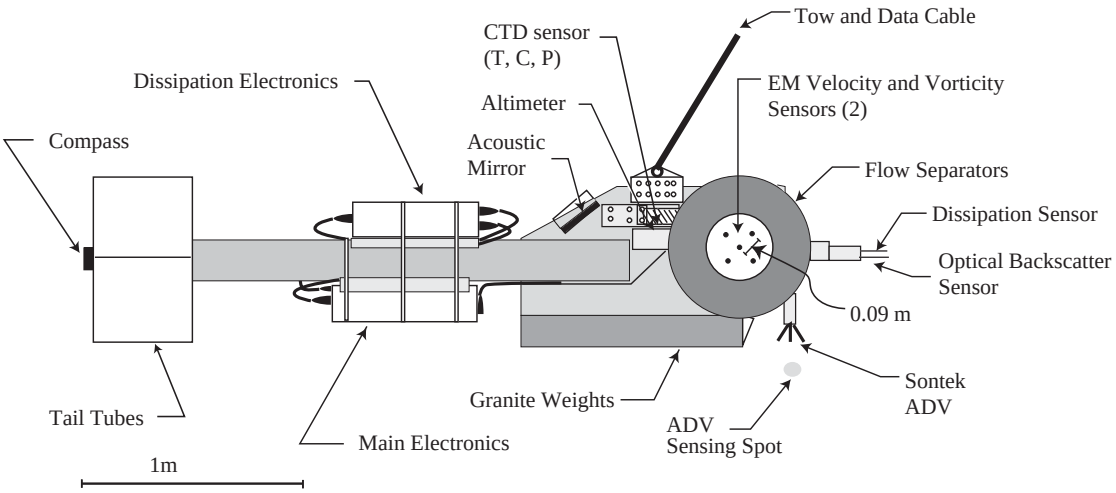

Fig. 3. Sketch of the EMVM and sensors.

for measuring turbulence kinetic energy dissipation rate, an optical backscattering sensor (OBS), and an acoustic Doppler velocimeter (ADV). The details of the sensors and measurements are described in Sanford et al. (1999).

The VM mounted on the side of the towed-body measured the vertical velocity, the streamwise velocity, and the spanwise vorticity. The VM mounted on the bottom of the towed-body measured the spanwise velocity, the streamwise velocity, and the vertical vorticity. A large tail on the EMVM towed-body oriented the vehicle into the dominant streamwise direction. Here, horizontal velocity components are defined according to the orientation of the EMVM towed-body; streamwise velocity u is in the direction of the towed-body, and spanwise velocity v is perpendicular to the towed-body.

The maximum ebb tidal current was 0.6–0.8 m s^{-1}. The background stratification and shear varied greatly during the five experiments (Fig. 4). These vertical profiles were computed using measurements taken when the EMVM was profiled vertically. The water was weakly stratified and sometimes nearly homogeneous in PP1 and PP2, and moderately to strongly stratified in PP3–5. Data taken in PP2 while the water was nearly homogeneous during the peak ebb tide were used to study the unstratified turbulent boundary layer (Sanford and Lien, 1999; Lien and Sanford, 2000).

Vertical profiles of shear square S^2 showed an order of magnitude increase near the bottom few meters. Above the bottom high-shear layer, the shear decreased in weakly stratified water and remained nearly constant in the moderately to strongly stratified water. These vertical profiles were averaged over $\sim\frac{1}{2}$ ebb tidal period centered on the peak ebb tidal current. There were significant temporal variations of stratification and shear. Small vertical-scale fluctuations of S^2 could have been smoothed out because we averaged S^2 over the half ebb tidal cycle at 0.5-m vertical resolution (Fig. 4).

Vertical profiles of Richardson number $Ri = N^2/S^2$ were close to or less than 1/4 (Fig. 4). During moderately and strongly stratified conditions, the Ri was within a factor of two from the critical value 1/4 above 3 mab (meters above bottom). This is consistent with a prediction of constant Ri by the local MO similarity scaling in the z-less regime (Nieuwstadt, 1984). During nearly homogeneous conditions, Ri is much less than 1/4.

In the following analysis, measurements taken at fixed depths will be used to study turbulence spectral properties and similarity scalings.

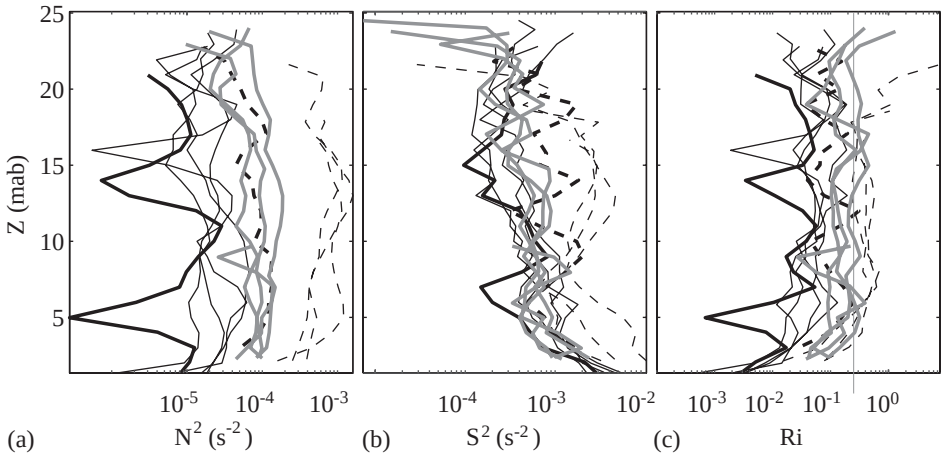

Fig. 4. Vertical profiles of (a) stratification (N^2), (b) shear-squared (S^2), and (c) gradient Richardson number (Ri) averaged over each day of each experiment (1 day in PP1, 4 days in PP2, 1 day in PP3, 3 days in PP4, and 3 days in PP5) as a function of meters above bottom (mab). In each day, 3–6 h of measurements were taken during the semidiurnal ebb tide. Vertical profiles of streamwise velocity and density were averaged in 0.5-m vertical bins. The thick solid curve represents the PP1, thin solid curves represent PP2, the thick dashed curve represents the PP3, thin dashed curves represent PP4, and gray curves represent PP5. The vertical line in panel (c) denotes $Ri = 1/4$.

Measurements taken while the EMVM was profiled vertically provide information on shear and stratification.

3. Spectral properties in a stable boundary layer

Extensive studies of turbulence spectral properties have been conducted in the atmospheric boundary layer, e.g., the 1968 Kansas experiment and the 1973 Minnesota experiment (Kaimal and Wyngaard, 1990). An understanding of the spectral details of the turbulence is vital to improve parameterizations of turbulent fluxes in numerical models.

In the neutral condition, spectral properties of the oceanic bottom boundary layer are consistent with those found in the atmospheric surface boundary layer (Lien and Sanford, 2000). In stratified flows, both internal waves and turbulence exist in the same physical and Fourier spaces. The turbulence mixing is suppressed and internal waves are enhanced by the stratification. Therefore, velocity spectral properties are significantly altered by the stratification.

Turbulence spectra have been summarized from previous studies of the atmospheric boundary layer (Kaimal and Finnigan, 1994); this summary is a guide for our analysis. In the inertial subrange, where the turbulence scale is much smaller than the scale of energy-containing eddies and much greater than the scale of viscous dissipation, velocity spectra follow the Kolmogorov scaling, i.e.,

$$\Phi_q(k_x) = c_q \alpha \varepsilon^{2/3} k_x^{-5/3}, \tag{1}$$

where Φ_q is the velocity spectrum, $q = u, v, w$ is the velocity component, k_x is the streamwise wavenumber, $\alpha = 1.5$ is the Kolmogorov constant, $c_q = 0.33$ for streamwise velocity, $c_q = 0.44$ for the spanwise and vertical velocity, and ε is the dissipation rate of turbulence kinetic energy (Sreenivasan, 1995). The spectral level in the inertial subrange is proportional to $\varepsilon^{2/3}$, which varies with the background forcing and stratification.

At scales larger than the inertial subrange, turbulence spectra cannot be determined by the theoretical similarity scaling. Kaimal (1973) compiled turbulence spectra observed in the stable

atmospheric boundary layer and found an empirical form

$$\frac{k\Phi_q(k)}{\sigma_q^2} = \frac{a(k/k_0^q)}{1 + a(k/k_0^q)^{5/3}}, \quad (2)$$

where k_0^q is a reference wavenumber. This empirical spectrum Φ_q has a $-\frac{5}{3}$ spectral slope at $k \gg k_0^q$, the inertial subrange, and is white at low wavenumbers. The constant $a = 0.164$ is fixed so that the integration of the spectrum Φ_q equals the total variance σ_q^2. The peak of the variance preserving spectrum $k\Phi_q$ is at $k_m^q = 3.77k_0^q$.

The empirical spectrum (2) is only valid for turbulence in the absence of internal waves and has to obey the Kolmogorov scaling in the inertial subrange (1). Consequently, a turbulence scaling is

$$\varepsilon = b_q \sigma_q^3 k_0^q, \quad (3)$$

where $b_q = (c_q\alpha)^{-3/2} = 2.87$, 1.87, and 1.87 for the streamwise, the spanwise, and the vertical velocities, respectively. A similar scaling has been concluded in previous studies. In highly energetic stratified oceanic turbulent flows, D'Asaro and Lien (2000) found a linear relationship between ε and the variance of vertical velocity σ_w^2, i.e.,

$$\varepsilon = C\sigma_w^2 N, \quad (4)$$

where the nondimensional constant $C = 0.3$–0.6. Weinstock (1981) proposed a similar relation with $C = 0.4$–0.5 in the stratosphere. Combining the vertical component of (3) and (4), we find $k_{Oz} = (4\text{–}11.4)k_0^w$. The Ozmidov wavenumber $k_{Oz} = \varepsilon^{-1/2}N^{3/2}$ is well known as the wavenumber of energy containing eddies for stratified turbulence. Therefore, Kaimal's empirical spectrum predicts the similar wavenumber for energy containing eddies, i.e., $k_m^w = 3.8k_0^w = (0.4\text{–}0.9)k_{Oz}$, similar to the Ozmidov wavenumber expected for free shear turbulence.

In the following, we present observed oceanic spectra of streamwise velocity and vertical velocity, compare them with (1) in the inertial subrange, normalize the observed spectra taken in a strongly stratified period by their variance, and fit the normalized spectra to (2) to determine k_0^w and k_0^u.

3.1. Observed spectra

Velocity spectra were computed using measurements taken at fixed depths. There was a total of 459 time segments. These measurements were taken mostly close to the bottom (76% below 9 mab) for detailed observations of turbulence in the bottom boundary layer and were often longer than 10 min. Some short segments, generally <3 min, were taken near the surface.

Typical streamwise and vertical velocity spectra observed during strong ebb tides are shown in Fig. 5. The streamwise velocity spectra exhibit a clear $-5/3$ spectral shape in the wavenumber range 0.3–4 m^{-1}, slightly more than a decade. At $k_x < 0.3\ \mathrm{m}^{-1}$, streamwise velocity spectra are slightly flatter than a $-5/3$ slope, and at $k_x > \sim 4\ \mathrm{m}^{-1}$, spectra drop steeper than a $-5/3$ slope as a result of sensor response (see Sanford et al., 1999). Vertical velocity spectra exhibit a white spectrum at $k_x < 1\ \mathrm{m}^{-1}$, a $-5/3$ spectral slope in 1–4 m^{-1}, and a steeper spectral roll-off at $k_x > 4\ \mathrm{m}^{-1}$ as a result of sensor response. These observed spectral shapes, excluding the high-wavenumber sensor roll-off, are consistent with Kaimal's empirical spectrum in the stable boundary layer, although they were taken in various stratification conditions.

To further evaluate the inertial subrange, we compared ε measured directly from the shear probe with ε estimated by observed velocity spectra in the inertial subrange. The shear probe samples at 400 Hz. Estimates of ε were computed by fitting the shear spectrum, measured by the shear probe, to the Nasmyth spectrum (Moum et al., 1995) in the wavenumber range between 2 and 150 cpm. The calibration procedure of shear probes is identical to that used for the shear probe mounted on the Advanced Microstructure Profilers explained in Moum et al. (1995). We have performed the shear-probe calibration before cruises, but not after cruises. Changing sensitivity of shear probes over time could introduce bias in estimates of ε.

Estimates of ε were also computed by multiplying the velocity spectra by $k_x^{5/3}$, identifying the inertial subrange (white), and averaging over the selected inertial subrange. The streamwise velocity

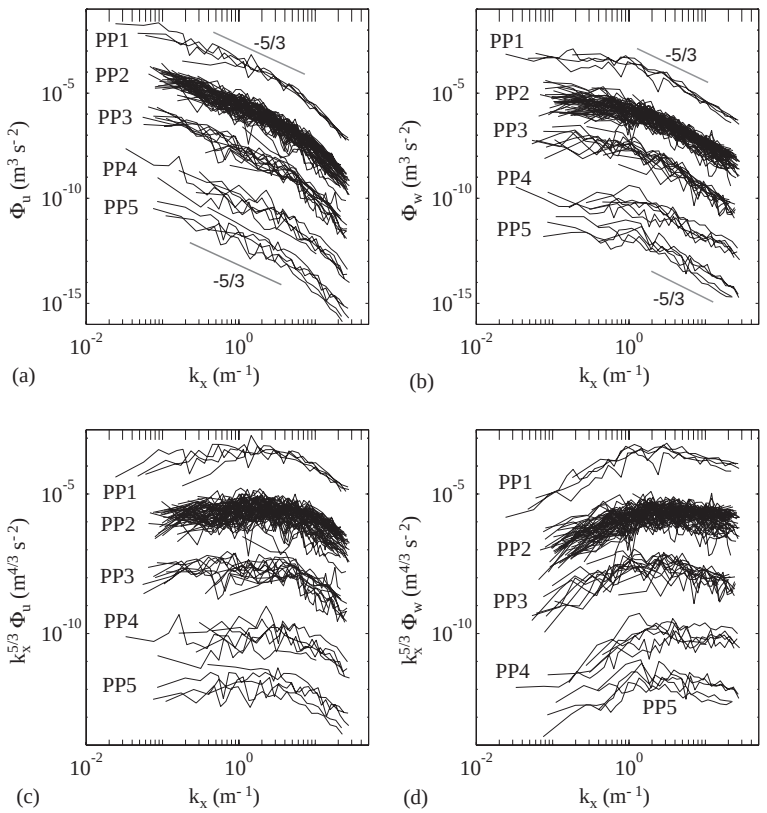

Fig. 5. Spectra of (a) streamwise velocity, and (b) vertical velocity observed during PP1, PP2, PP3, PP4, and PP5. Only spectra taken during the strong ebb tide, $U > 0.4$ m s^{-1}, are shown. In (c) and (d) spectra are multiplied by $k_x^{5/3}$, where k_x is the streamwise wavenumber, so that the inertial subrange appeared as white for the convenience of estimating the dissipation rate of turbulence kinetic energy. Spectral levels are offset by $10^{-2}, 10^{-4}, 10^{-6}$, and 10^{-8} for PP2, PP3, PP4, and PP5, respectively. Spectral slopes of $-5/3$ are indicated in (a) and (b).

spectrum generally had its inertial subrange extended to a lower wavenumber than the vertical velocity spectrum (Fig. 5). Consequently, ε estimated from the vertical velocity spectrum was noisier than that estimated from the streamwise velocity spectrum (Fig. 6). Nevertheless, a good correlation was found between ε measured from the shear probe and ε estimated by velocity spectra. The ε measured from the shear probe was about twice that computed from the velocity spectra. Possible reasons for this discrepancy are (1) inaccurate estimates of ε in the inertial subrange or (2) inaccurate calibration of the shear probe. Non-steadiness of the mean current does not contribute a large bias to our estimates of ε because the mean current remained nearly constant in the typical 2-min segments of time series used to compute spectra. We suspect that the discrepancy is due to the change of sensitivity of shear probes.

3.2. Universal spectral form?

Kaimal (1973) compiled spectra from the Kansas experiment and found a universal spectral form (2) for turbulent velocity in a stable atmospheric boundary layer. Removing internal gravity waves from observed measurements is not a trivial task. In the analysis of turbulence in a stable atmospheric boundary layer, Nieuwstadt (1984)

successfully removed effects of internal waves by (1) choosing measurements taken during periods of strong turbulence, (2) choosing measurements when velocity variances decrease with altitude, and (3) low-pass filtering of the measurements. The benefit of (1) is obvious. The second scheme assumes the boundary is the source of turbulence. The third procedure assumes that there is a spectral gap between internal waves and turbulence. Supports for (2) and (3) were found by Caughey et al. (1979) in a weakly stable boundary layer. In a very stable boundary layer, enhanced turbulence, generated by processes such as breaking internal waves, was sometimes found detached from the boundary (Mahrt, 1999). In this circumstance, the spectral gap between internal waves and turbulence might not exist. Therefore, in a very stable boundary layer it is nontrivial to completely exclude effects of internal waves from measurements by applying procedures (2) and (3).

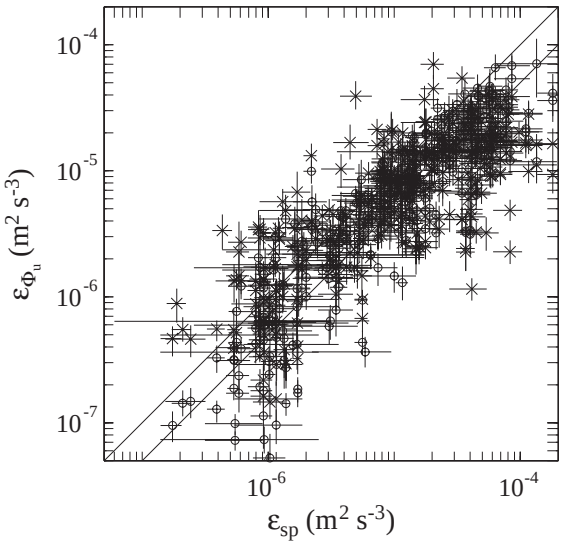

Fig. 6. Comparison of ε observed from the shear probe ε_{sp} and ε_{Φ_u} estimated from the observed spectra of streamwise velocity (circles), and vertical velocity (Xs). Vertical and horizontal lines represent 95% confidence intervals for the estimated and observed ε, respectively. Two diagonal lines represent the $\varepsilon_{sp}/\varepsilon_{\Phi_u} = 1$ and 2, respectively.

To search for a similar universal spectrum (1973) for the oceanic stratified bottom boundary layer, we used measurements taken on 19 November 1998 during the PP5 experiment. These measurements were chosen because they were taken at fixed depths in a stratified flow for a relatively longer period, nominally at 1.6, 3.6, 5.6, and 7.6 mab, for typically 14 min (Fig. 7). Within each fixed-depth segment, there were occasional rapid changes of depth due to winch motion. We label the segments according to the period when

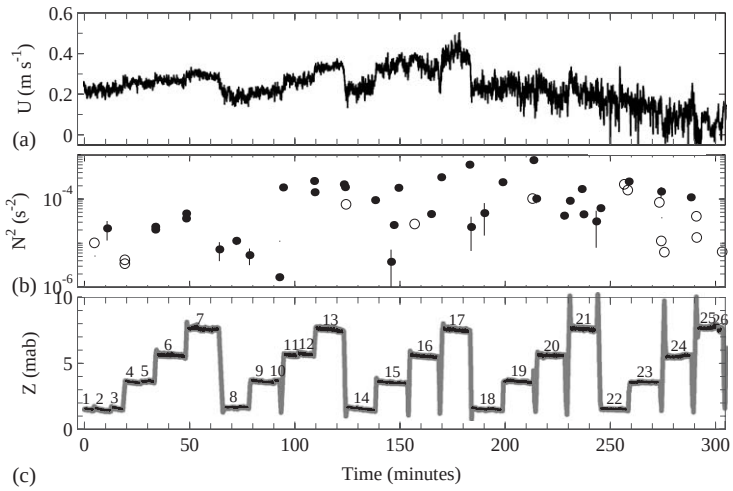

Fig. 7. Time series of (a) streamwise velocity, (b) buoyancy frequency-squared N^2, and (c) altitude (distance above the bottom) of the EMVM on 19 November 1998 during PP5. The N^2 was computed using the profiling data. N^2 values before and after measurements at fixed depths are shown. Open circles indicate negative N^2. In panel (c) labels denote the segment numbers.

the EMVM was relatively steady at a fixed depth (see labels in Fig. 7c). Between fixed-depth segments, the EMVM was profiled to measure vertical stratification and shear. Estimates of N^2 closest to the time of fixed-depth segments are shown in Fig. 7b. The water was nearly homogeneous within the first 0.5 h, $N^2 \leqslant 3 \times 10^{-5}$ s^{-2} for 1.5 h, $N^2 \geqslant 10^{-4}$ s^{-2} for $\sim$2 h when the ebb tidal current increased, and became nearly homogeneous within the last hour of measurements when the tidal current began to reverse. The tidal speed during the peak tide was $\sim$0.4 m s^{-1} at 7.6 mab.

Note that the stratification was highly variable in time and with depths. As an example, three vertical profiles of density and streamwise velocity taken within 15 min before and after segment 17 are shown in Fig. 8. The first two profiles, taken within 1 min, showed a similar density structure but significantly different velocity structure. The third profile, taken $\sim$15 min later, exhibited a very different density structure. The compass of the EMVM showed that the orientation of the mean flow rotated in depth and varied in time. These profiles were averaged at 1-s intervals, corresponding to 0.1–0.2 m in the vertical with the typical profiling speed of 0.1–0.2 m s^{-1}. Both velocity and density profiles showed small vertical scale, $<$1 m, fluctuations embedded in the background profiles. Steps of constant density and small-scale overturning were present. Similar complex vertical structures have been observed in the stratified atmospheric boundary layer. Chinomas (1999) suggested that these fine scale steps play crucial roles in triggering shear instability.

In the turbulent boundary layer, turbulence properties are strongly modified by background shear and stratification. Because of the aforementioned complex variability of shear and stratification, we expect that turbulence properties will vary at the similar time scale. The variation of vertical velocity spectra is illustrated with the $\sim$14-min measurements taken at 7.5 mab, segment 17, when the ebb tidal current reached its maximum value of $\sim$0.4 m s^{-1} (Fig. 9). During this period, ε was 2×10^{-7}–2×10^{-5} W kg^{-1}, U was 0.29–0.51 m s^{-1}, and w was $\pm$0.06 m s^{-1}. The mean vertical velocity variance σ_w^2 was 3×10^{-4} m^2 s^{-2}, but reached to 10^{-3} m^2 s^{-2} occasionally.

We performed a wavelet analysis on the vertical velocity using the Daubechies' least asymmetric filter of length 8 (Percival and Walden, 2000). The linear phase shift due to the asymmetry of the wavelet filter has been corrected. Most of vertical velocity variance was contributed by eddies of wavenumber $k_x \approx 1$ m^{-1}, ranging between 0.5 and 10 m^{-1} (white shading). The Ozmidov wavenumber $k_{Oz} = N^{3/2}\varepsilon^{-1/2}$ is $\sim$1.5 m^{-1} giving ε of $\sim 5 \times 10^{-6}$ W kg^{-1}, and N^2 of $\sim 5 \times 10^{-4}$ s^{-2}. Vertical velocity spectra varied significantly in time.

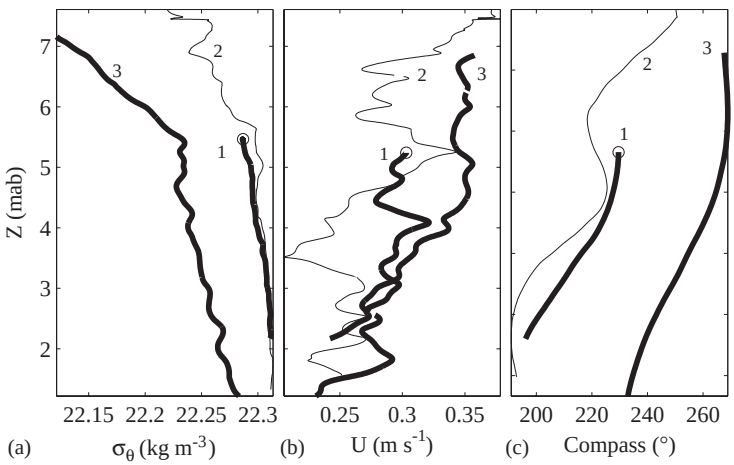

Fig. 8. Vertical profiles of (a) density, (b) streamwise velocity, and (c) compass of the EMVM taken before (profiles 1 and 2) and after (profile 3) segment 17 (see Fig. 7).

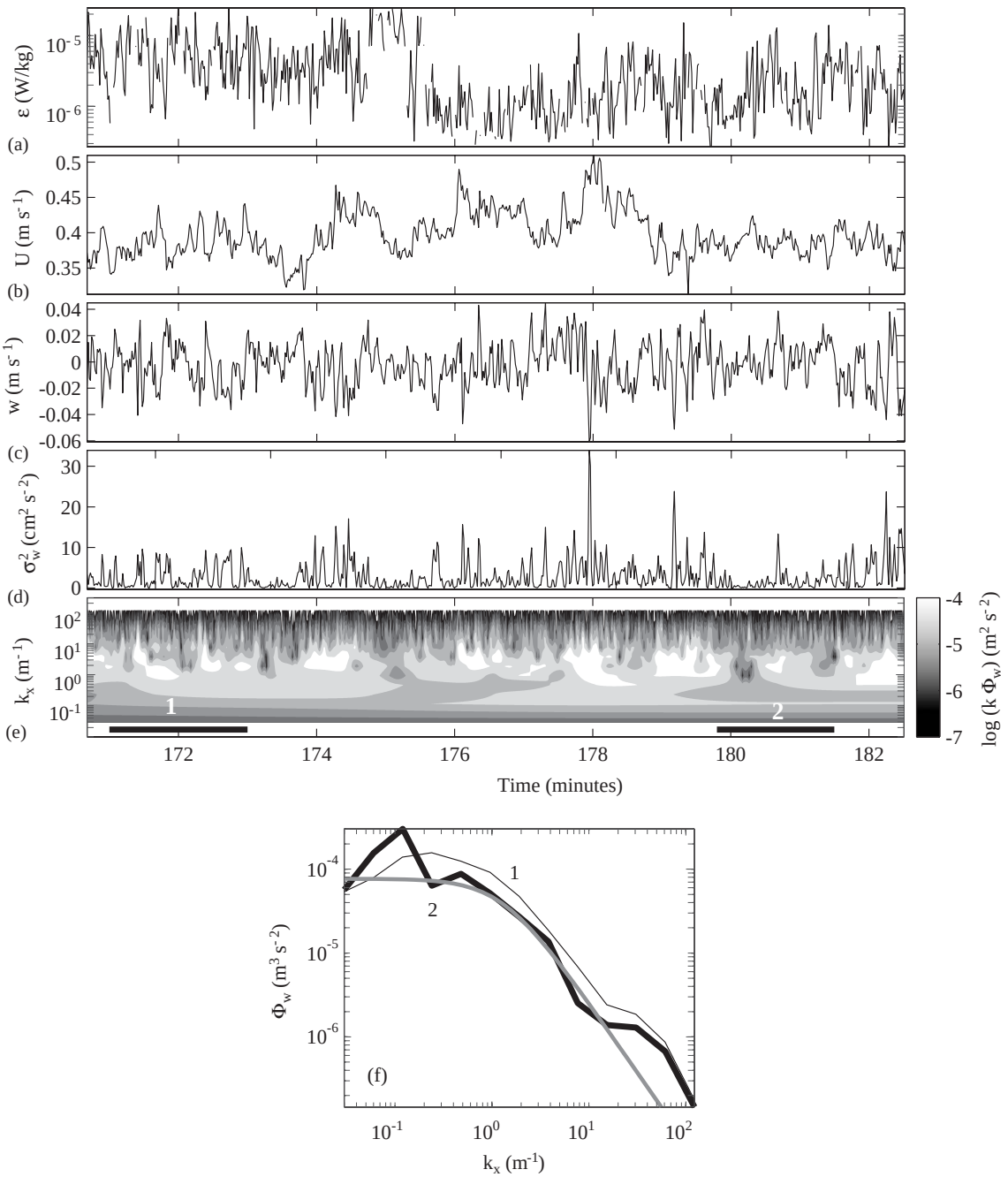

Fig. 9. Time series of (a) ε, (b) streamwise velocity U, (c) vertical velocity w, and (d) variance of w averaged in 1-s interval during the segment 17. The gray-scale shading in (e) shows the variance preserving plot of vertical velocity as a function of time and wavenumber computed by wavelet analysis. Two horizontal thick bars at the bottom of (e) mark the two time periods when the vertical velocity spectra shown in (f) were computed using results from the wavelet analysis. The gray curve in (f) represents Kaimal's model spectrum (Eq. (2)) assuming $\sigma_w^2 = 2 \times 10^{-4}$ m^2 s^{-2}, and $k_0^w = 0.5$ m^{-1}.

Examples of two vertical velocity spectra computed by averaging 2 min of wavelet spectra ~9 min apart show that spectral levels change by a factor of two in the inertial subrange, consistent with the change of ε. Between k_x of 0.2 and 20 m^{-1}, spectral shapes seem to resemble Kaimal's model spectrum, white at low wavenumbers and $-5/3$ in inertial subrange. Below 0.2 m^{-1}, spectral levels elevate presumably due to non-turbulent motions. The elevated spectral level at $k_x \geqslant 20$ m^{-1} is likely due to over-correction by the sensor response (Sanford et al., 1999).

Our observed spectra do not show a clear spectral gap between internal waves and turbulence as found in the atmospheric boundary layer (Caughey et al., 1979). To remove effects of internal waves, we examine individual spectra, carefully exclude low-wavenumber spectra where spectral levels are elevated above the background white spectrum, and exclude high-wavenumber spectra where noise spikes are present. After the above procedure, 4 of 26 vertical velocity spectra were removed. The remaining 22 velocity spectra were of a similar shape, but the levels differed by nearly two decades (Fig. 10). These spectra were fitted to Kaimal's model spectrum (2) to obtain k_0^w. The estimates of k_0^w vary between 0.26 and 0.64 m^{-1} with a mean of 0.48 m^{-1}. The corresponding estimates of k_m^w are 1–2.5 m^{-1}.

We normalized observed spectra by their variances and normalized wavenumbers by estimated k_0^w. This normalization procedure reduces the range of spectral levels to a factor of 5. The mean of normalized spectral shape resembles Kaimal's model spectrum. However, the observed normalized spectrum slightly exceeds the model spectrum below the inertial subrange, $k_x \leqslant 10\ k_0^w$, and at $k_x \geqslant 30\ k_0^w$. We suggest that the extra energy below the inertial subrange is due to the combination of internal waves and turbulence. Internal waves and turbulence exist at the same scales. Within these common wavenumbers, it is impossible to remove internal waves from observations on the basis of characteristics of wavenumber spectra. The extra energy at high wavenumbers is due to spurious velocity noise produced during depth changes and cable strumming which was not completely removed.

The same analysis was applied to the streamwise velocity spectra. Only 20 of the 26 streamwise velocity spectra exhibited a clear inertial subrange (Fig. 11). Spectral levels varied by ~1.5 decades. Fitting these spectra to Kaimal's model spectrum yields k_0^u of 0.03–0.2 m^{-1}, with a mean of 0.08 m^{-1}. The ratio between the means of our estimates of k_0^u and k_0^w is 1/6, close to the 1/8 found in the stable atmospheric boundary layer (Moraes and Goedert, 1988). The corresponding wavenumber of the spectral peak is $k_m^u \approx 0.3$ m^{-1}. Because our spectra were computed with measurements about 10-min long, observed streamwise velocity spectra barely resolve wavenumbers below

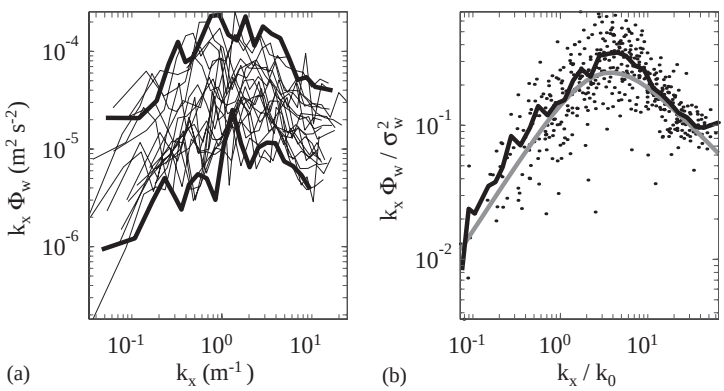

Fig. 10. (a) Observed vertical velocity spectra and (b) normalized vertical velocity spectra (dots). The two thick solid curves in (a) show two spectra with significantly different spectral levels. The thick solid curve in (b) shows the mean of the observed normalized spectra and the thick gray curve is Kaimal's model spectrum (Kaimal, 1973).

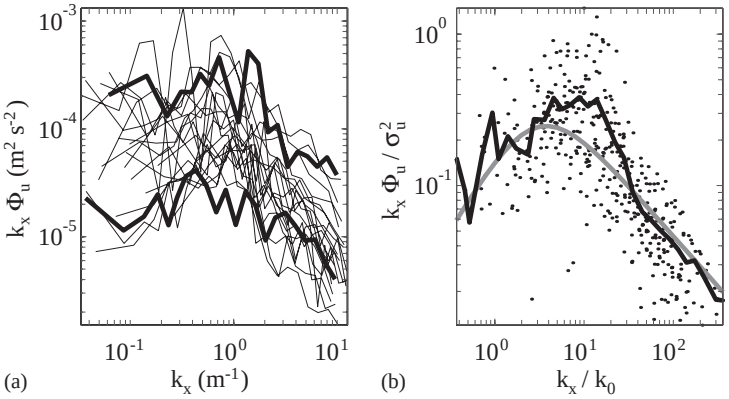

Fig. 11. (a) Observed streamwise velocity spectra and (b) normalized streamwise velocity spectra (dots). The two thick solid curves in (a) show two spectra with significantly different spectral levels. The thick solid curve in (b) shows the mean of the observed normalized spectra and the thick gray curve shows the model spectrum presented by Kaimal (1973).

$0.05\ \mathrm{m}^{-1}$. Our estimates of k_0^u could be overestimated.

The streamwise velocity variance was about four times the vertical velocity variance, close to the ratio of 3 found in the stable atmospheric boundary layer (Kaimal, 1973). The observed higher ratio is possibly due to contributions from internal waves, which are mostly dominated by horizontal velocity variance. Because the spectral peak of the streamwise velocity is at a wavenumber, $k_m^u \approx 0.3\ \mathrm{m}^{-1}$, not much greater than the smallest resolvable wavenumber, $\sim 0.05\ \mathrm{m}^{-1}$, it is difficult to identify the white-spectrum regime below k_m^u and to remove elevated variances at low wavenumbers contributed by internal waves. Consequently, we believe that observed streamwise velocity spectra are significantly contaminated by internal waves.

Normalizing streamwise velocity spectra by variances and wavenumbers by k_0^u slightly collapses spectra in the inertial subrange, but the spread at the spectral peak is still about one decade. The mean normalized spectrum has a similar spectral level to Kaimal's model, except near the spectral peak where the observed spectrum is twice that of Kaimal's.

Overall, spectra observed in the stratified oceanic bottom boundary layer show some agreement with Kaimal's model spectrum in the inertial subrange. However, there are significant departures at wavenumbers below the inertial subrange, which are likely due to the presence of internal waves. The discrepancy is greater for the horizontal than for the vertical motion. This is consistent with the hypothesis of internal wave contamination because internal waves are dominated by the horizontal motion. Our spectral selection procedure appears ineffective at removing internal waves. The major obstacle is that no clear spectral gap exists between internal waves and turbulence in the oceanic stratified turbulent boundary layer.

4. Similarity scaling

In the very stable atmospheric boundary layer, enhanced turbulence is often found in layers of enhanced shear and reduced Ri with little dynamic connection with the boundary (Finnigan, 1999). In other words, turbulence in the very stable atmospheric boundary layer may resemble free shear stratified turbulence. Both Reynolds stress and buoyancy flux are required to examine the local similarity scaling. Our velocity and CTD sensors are separated by 0.5 m, which results in inaccurate estimates of buoyancy flux.

The scaling of turbulence kinetic energy dissipation rate ε could be established on the basis of previous studies of shear turbulence. In the z-less stable boundary layer, Nieuwstadt (1984) shows

that $\sigma_w^2 \approx -2\langle u'w' \rangle$ and $Ri \approx 1/4$, i.e., the shear $d_z U \approx 2N$. Assuming a local balance between the shear production and the turbulence kinetic energy dissipation, i.e, $\varepsilon \approx -\langle u'w' \rangle d_z U$, yields a scaling law $\varepsilon \approx \sigma_w^2 N$. This scaling is similar to that proposed by Gargett (1984), Weinstock (1981), and D'Asaro and Lien (2000).

Among oceanic microscale researchers, the diapycnal diffusivity K_ρ is often computed as $K_\rho = 0.2\varepsilon N^{-2}$ (Osborn, 1980). Assuming the turbulent Prandtl number of 1, a similarly scaling $\varepsilon \approx 0.84\sigma_w^2 N$ is deduced on the basis of Nieuwstadt's (1984) result of $\sigma_w^2 \approx -2\langle u'w' \rangle$ and Osborn's (1980) expression for diapycnal diffusivity.

Matching Kaimal's model spectrum with the Kolmogorov similarity scaling in the inertial subrange produces a relation $\varepsilon = 1.87\sigma_w^3 k_0^w = 0.5\sigma_w^3 k_m^w$. Assuming $k_m^w = k_{Oz} = N^{3/2}\varepsilon^{-1/2}$, a similar scaling of ε is obtained as $\varepsilon = 0.62\sigma_w^2 N$.

The above discussion demonstrates that three independent approaches arrive at a common scaling for ε in the shear stratified turbulent flows. Kaimal's model spectrum for boundary-layer turbulence is consistent with results of stratified free shear turbulence assuming the Ozmidov scale is the scale of energy-containing eddies.

Our observations show a clear correlation between ε and σ_w^2 spanning nearly 1.5 decades (Fig. 12). Unfortunately, no simultaneous measurements of ε and N were taken. Therefore, only measurements taken during the period of nearly steady stratification $N_0 \approx 0.02\ \mathrm{s}^{-1}$, segments 11–21, are plotted. This period corresponds to the peak tidal flow and the strongest stratification. ε and σ_w^2 were computed over 40-s intervals. This time interval was chosen because it is sufficiently long to capture vertical velocity variance of turbulence and it is short enough to retain the temporal variation of ε and σ_w^2. For a typical mean streamwise velocity exceeding $0.3\ \mathrm{m\ s}^{-1}$, the 40-s time interval allows the smallest resolvable wavenumber of $0.5\ \mathrm{m}^{-1}$. This is sufficient to capture most of the vertical velocity variance.

The mean ratio of ε and σ_w^2 is $0.03\ \mathrm{s}^{-1}$, i.e., $\varepsilon \approx 1.5 N_0 \sigma_w^2$. This is about a factor of three greater than the scaling based on Kaimal's model spectrum and the Ozmidov scaling. Assuming that the observed ε is overestimated by a factor of two (see 3.1), yields a relation of $\varepsilon_{adj} \approx 0.75 N_0 \sigma_w^2$, where $\varepsilon_{adj} = 0.5\varepsilon$. In summary, $\varepsilon = 1.1 \pm 0.4 N_0 \sigma_w^2$.

A 40-s averaging time interval was also used to find the relation between vertical velocity variance and the momentum flux. A good correlation between σ_w^2 and $\langle u'w' \rangle$ was found (Fig. 12). The computed momentum flux $\langle u'w' \rangle$ is occasionally positive, but the mean is negative. The ratio between σ_w^2 and $\langle u'w' \rangle$ suggests a relation $\sigma_w^2 \approx -4\langle u'w' \rangle$. The proportionality 4 is greater than Nieuwstadt's result of 2. This may be due to the effects of internal waves. Note that observations of

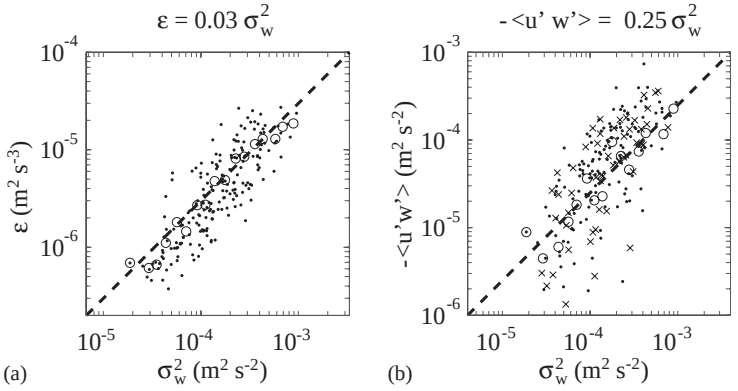

Fig. 12. Scatter plots of (a) turbulence kinetic energy dissipation rate ε vs. variance of vertical velocity σ_w^2, and (b) momentum flux $-\langle u'w' \rangle$ vs. σ_w^2. Small dots are original data. The crosses in (b) are data of $\langle u'w' \rangle > 0$. Open circles are average values of ε and $-\langle u'w' \rangle$ in grid-bins of σ_w^2. The dashed line in (a) represents the mean ratio between ε and σ_w^2, and the dashed line in (b) represents the mean ratio between $-\langle u'w' \rangle$ and σ_w^2.

Caughey et al. (1979) exhibited a similar higher ratio (Fig. 2 of Nieuwstadt (1984)).

5. Discussion

5.1. Spectral gap

In stratified oceanic flows internal waves are often more energetic than the turbulence. We believe that both internal waves and turbulence exist in our observations. The purpose of this section is to illustrate the difficulty of separating internal waves and turbulence in the stratified oceanic boundary layer. This difficulty may have contributed to the discrepancy between our observed velocity spectra and the universal turbulence spectra found in the atmosphere. However, the discrepancy may also be due to eddies, and effects of advection and non-stationarity. These processes are beyond the scope of this study and will not be discussed.

Within the stable atmospheric boundary layer, a spectral gap at ~ 0.01 Hz has been observed separating low-frequency internal waves and high-frequency turbulence (Caughey et al., 1979). To study the turbulent boundary layer, internal wave energy at frequencies below the spectral gap is filtered (e.g., Caughey et al., 1979; and Nieuwstadt, 1984).

Our observed spectra of velocity components do not show a spectral gap separating internal waves and turbulence. Therefore, it is difficult to distinguish between internal waves and turbulence using velocity spectra. Caughey (1984) pointed out that at higher levels of the stable atmospheric boundary layer, the spectral gap might disappear because, with the increasing buoyancy frequency, the spectral peak of internal waves moves closer toward the peak of turbulence. In the surface boundary layer, the wavenumber of the spectral peak of turbulence velocity decreases with altitude and is independent of the buoyancy frequency.

A discernible spectral gap requires that internal waves and turbulence have their spectral peaks at separate wavenumbers, or frequencies, and that they have comparable energy (Fig. 13). If the energy of internal waves E_{iw} increases, the spectral peak of turbulence may be overwhelmed by the internal wave spectrum Φ_{iw} and become indiscernible even though the dominant wavenumbers for internal waves and turbulence, k_{iw} and k_m, are separated. The spectral gap also becomes indiscernible if the peaks of two spectra move closer (Caughey, 1984).

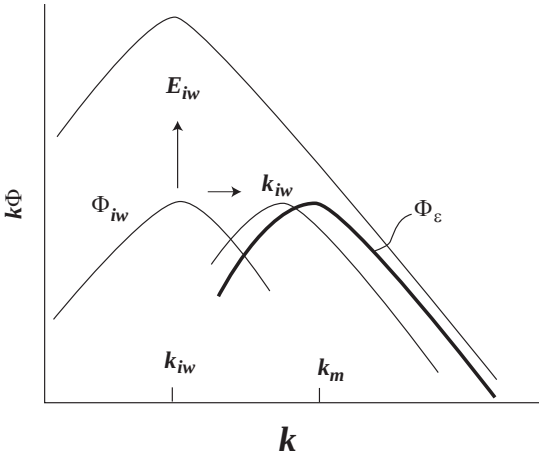

Fig. 13. Diagram illustrating spectral gap between internal waves and turbulence. Three thin curves represent velocity spectra of internal waves Φ_{iw} and the thick curve represents the velocity spectrum of turbulence Φ_ε. The wavenumber of the peak of Φ_{iw} is denoted as k_{iw} and the wavenumber of the peak of Φ_ε is denoted as k_m.

In the strongly stratified oceanic bottom boundary layer, the k_{iw} may depend on the bottom topography, the background shear and buoyancy frequency for shear instability flows, and the water depth. The energy level of Φ_{iw} should vary with the shear of the tidal flow and the buoyancy frequency; both are highly variable in time. Our observations taken in PP5 were in a strongly stratified regime where the Ozmidov scale was $O(1\text{ m})$. These observations were likely in the local-similarity-scaling layer and the z-less layer. In these regimes, the spectral peak k_m depends less on the boundary and more on the stratification and the local flux. We suggest that k_m is equivalent to the Ozmidov wavenumber $k_{Oz} = N^{3/2}\varepsilon^{-1/2}$. In the energetic shear-stratified bottom boundary layer, intermittent wave breaking supplies energy to turbulence. Therefore, ε as well as k_{Oz} depend on N, the shear, and the internal-wave energy.

At the observation site there were broad-crested ripples on the bottom of ~0.3-m height, ~16-m wavelength, and ~100-m crest length. For internal waves generated at the bottom, the dominant wavenumber k_{iw} is about 0.4 m^{-1}. This is close to the typical Ozmidov wavenumber $O(1\ m^{-1})$ in our observations. This might also explain the absence of a spectral gap between internal waves and turbulence in our observed velocity spectra.

5.2. Separating internal waves and turbulence using potential vorticity

In the Lagrangian frequency domain, internal waves and turbulence may be separated by the buoyancy frequency N (D'Asaro and Lien, 2000). The stratified flow can be represented as the superposition of isotropic turbulence at Lagrangian frequencies greater than N and anisotropic, internal waves of dominantly horizontal motion at Lagrangian frequencies below N. Thus internal waves and turbulence may be separated in the Lagrangian frame.

In the wavenumber or Eulerian frequency domain, separating internal waves and turbulence is impossible if a spectral gap does not exist. In flows undergoing strong shear-instability, internal waves and turbulence are coupled, and there exists no clear separation between them.

Theoretically, there are distinct characteristics distinguishing internal waves from turbulence. Linear internal waves are governed by a dispersion relation. The energy of internal waves exists dominantly in a specific wavenumber-frequency domain. As the nonlinearity increases, the energy begins to spread about the dispersion curve (Holloway, 1983). In contrast, turbulence does not have a dispersion relation because it is strongly nonlinear. Therefore, one may extract the energy of internal waves following the dispersion curve, and extract energy of turbulence away from the dispersion curve of linear internal waves. Unfortunately, this requires taking time-series measurements over 3-D spatial scales covering the complete internal wave spatial and time scales. This is not feasible with the current technology.

Lien and Müller (1992a) presented consistency tests for spectral properties of internal waves and vortical motions in the ocean. The vortical motion carries the potential vorticity, defined as the inner product of the vorticity vector and the density gradient, and the internal wave has no fluctuating potential vorticity. Turbulence represents the vortical motion at small scales. It often has strong vortex stretching across the isopycnal surface. Lien and Müller (1992b) present a scheme to separate the energy of observed small-scale motions into internal waves and vortical modes. The scheme requires measurements of components of potential vorticity and works only in the linear to weakly nonlinear domain. Nevertheless, measuring the components of potential vorticity may be one of the effective ways to separate internal waves and turbulence.

The VMs measured both the vertical and spanwise components of vorticity. Simultaneous density gradients were not measured, so an estimate of the potential vorticity was not possible. Spectra of vorticity components computed using measurements taken in segment 17 are shown in Fig. 14. Observed vorticity spectra are in good agreement with those of isotropic turbulence after applying the sensor response function. The sensor

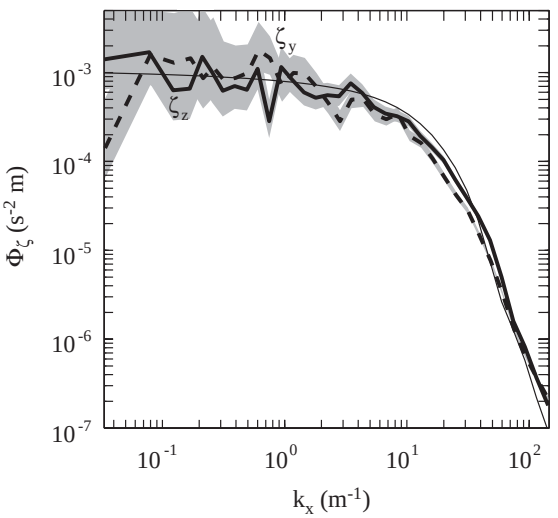

Fig. 14. Comparison of spectra of observed vertical vorticity (black solid curve) and spanwise vorticity (dashed curve) computed from measurements taken at the segment 17 (see Fig. 7). The thin solid curve is the theoretical vorticity spectrum of isotropic turbulence applying the sensor response function of the VM. Shading denotes the 95% confidence interval.

response function of vorticity measurements taken by the VM is discussed by Sanford and Lien (1999). The two vorticity spectra are not significantly different within the 95% confidence interval.

There is a hint that the vertical component of vorticity is slightly weaker than the horizontal component in the wavenumber between 0.1 and 1 m^{-1}, but the difference is not statistically significant. If isopycnal surfaces are flat, a vanishing vertical component of vorticity would imply zero potential vorticity, a signature of internal waves. However, small-scale internal waves have significant isopycnal tilts and the vertical component of vorticity could not be used as a surrogate of the potential vorticity. Therefore, our vorticity spectral analysis does not provide a conclusive proof of the existence of internal waves below the inertial subrange.

6. Summary

Turbulence velocity spectra in a stably stratified oceanic bottom boundary layer were examined. In a strongly stratified turbulent boundary layer separation of internal waves and turbulence remains an unsolved issue. Individual profiles of streamwise velocity and density show very complex vertical structure; small-scale steps, internal waves, and turbulence are present. Wavelet analysis shows significant variations of velocity spectra. Low-wavenumber spectral plateaus are ascribed to internal waves.

After carefully removing potential internal waves at low wavenumbers and instrumental noise at high wavenumbers, the observed spectra were normalized by their variances and compared with the canonical spectrum summarized from observations in the Kansas experiment (Kaimal, 1973). Our normalized spectra of vertical and streamwise velocity components agree with Kaimal's model spectrum in the inertial subrange. The reference wavenumber k_0 is estimated to be 0.48 and 0.08 m^{-1} for the vertical velocity and streamwise velocity spectra, respectively. The ratio between k_0^w and k_0^u is 6, close to that found in the atmospheric boundary layer.

At sub-inertial wavenumbers, observed spectra of vertical and streamwise velocity consistently exceed Kaimal's model spectra. Probable reasons for this discrepancy are (1) the contamination of internal waves, (2) inaccurate estimates of k_0, (3) inaccurate estimates of velocity variances, and (4) non-stationarity effects of turbulence. If internal waves and turbulence coexist at scales greater than the inertial subrange, there is no apparent method to separate one from the other in the velocity spectrum. The estimate of k_0 is sensitive to the spectral shape and variance. Furthermore, the variance of streamwise velocity could be underestimated for some short-record measurements that do not resolve large-scale eddies.

We propose that the parameter $k_m = 3.77k_0$ in Kaimal's model spectrum is related to the Ozmidov wavenumber k_{Oz}. Because we lack simultaneous estimates of N and ε during measurements at fixed depths, a direct correlation between k_m and k_{Oz} cannot be confirmed.

A relation $\varepsilon \approx 0.75\sigma_w^2 N$ was found when the water was strongly stratified. This is also consistent with Kaimal's model spectrum and $k_m = k_{Oz}$. This scaling has been proposed by previous studies of wall-free shear-driven turbulence (Gargett, 1984; Weinstock, 1981; D'Asaro and Lien, 2000). Our results support the hypothesis that turbulence properties in the very stably stratified boundary layer are analogous to the free shear turbulence (Fig. 3).

A correlation was found between momentum fluxes and vertical velocity variances. The proportionality was slightly different from the result of Nieuwstadt (1984). This result also reconciles the scaling of ε, the local balance between shear production and turbulence dissipation, and the critical Richardson number.

The strong stratification in the observed tidal bottom boundary layer is maintained by the advective density gradient. Our results, thereby, include effects of the horizontal advection.

The parameterization of turbulence in a strongly stratified turbulent boundary layer is complicated by the existence of internal waves. As concluded by Nappo and Johansson (1999), separating internal waves and turbulence requires more theoretical and observational studies. There is a

possibility of separating internal waves and turbulence on the basis of potential vorticity. Therefore, observations of potential vorticity will be needed to improve our understanding and parameterization schemes of turbulence in strongly stratified flows. Future studies should focus on the details and parameterizations of wave/turbulence interactions in the stratified turbulent boundary layer.

Acknowledgements

The successful observations taken in Pickering Passage were achieved with the vital help of John Dunlap, James Carlson, Eric Boget, and Gordon Welsh. Discussions with Eric Kunze and Eric D'Asaro have been very helpful. Comments of two anonymous reviewers were constructive and improved the presentation of our results. This research was supported by the Office of Naval Research. The authors are grateful for the long-duration support which proved vital to the development and use of the EMVM.

References

Anis, A., Moum, J.N., 1995. Surface wave-turbulence interaction: scaling $\varepsilon(z)$ near the sea surface. Journal of Physical Oceanography 25, 2025–2045.

Businger, J.A., Wyngaard, J.C., Izumi, Y., Bradley, E.F., 1971. Flux-profile relationships in the atmospheric surface layer. Journal of the Atmospheric Sciences 28, 181–189.

Caughey, S.J., 1984. Observed characteristics of the atmospheric boundary layer. In: Nieuwstadt, Dop (Eds.), Atmospheric Turbulence and Air Pollution Modeling. D. Reidel Publishing Company, Holland, 358pp.

Caughey, S.J., Wyngaard, J.C., Kaimal, J.C., 1979. Turbulence in the evolving stable layer. Journal of the Atmospheric Sciences 36, 1041–1052.

Chinomas, G., 1999. Steps waves and turbulence in the stably stratified planetary boundary layer. Boundary-Layer Meteorology 90, 397–421.

D'Asaro, E.A., Lien, R.-C., 2000. Lagrangian measurements of waves and turbulence in stratified flows. Journal of Physical Oceanography 30, 641–655.

Drennan, W.M., Donelan, M.A., Terray, E.A., Katsaros, K.B., 1996. Oceanic turbulence dissipation measurements in SWADE. Journal of Physical Oceanography 26, 808–815.

Finnigan, J.J., 1999. A note on wave-turbulence interaction and the possibility of scaling the very stable boundary layer. Boundary-Layer Meteorology 90, 529–539.

Gargett, A.E., 1984. Vertical eddy diffusivity in the ocean interior. Journal of Marine Research 42, 359–393.

Gemmrich, J.R., Farmer, D.M., 1999. Observations of the scale and occurrence of breaking surface waves. Journal of Physical Oceanography 29, 2595–2606.

Holloway, G., 1983. A conjecture relating oceanic internal waves and small-scale processes. Atmospheric-Ocean 21, 107–122.

Kaimal, J.C., 1973. Turbulence spectra, length scales and structure parameters in the stable surface layer. Boundary-Layer Meteorology 4, 289–309.

Kaimal, J.C., Finnigan, J.J., 1994. Atmospheric Boundary Layer Flows. Oxford University Press, New York.

Kaimal, J.C., Wyngaard, J.C., 1990. The Kansas and Minnesota experiments. Boundary-Layer Meteorology 34, 31–47.

Lien, R.-C., Müller, P., 1992a. Consistency relations for gravity and vortical modes in the ocean. Deep-Sea Research 39, 1595–1612.

Lien, R.-C., Müller, P., 1992b. Normal-mode decomposition of small-scale oceanic motions. Journal of Physical Oceanography 22, 1583–1595.

Lien, R.-C., Sanford, T.B., 2000. Spectral characteristics of velocity and vorticity fluxes in an unstratified turbulent boundary layer. Journal of Geophysical Research 105, 8659–8672.

Mahrt, L., 1999. Stratified atmospheric boundary layers. Boundary-Layer Meteorology 90, 375–396.

McWilliams, J.C., Sullivan, P.P., Moeng, C.H., 1997. Langmuir turbulence in the ocean. Journal of Fluid Mechanics 334, 1–30.

Mellor, G.L., Yamada, T., 1982. Development of a turbulence closure model for geophysical fluid problems. Reviews of Geophysics and Space Physics 20, 851–875.

Monin, A.S., Obukhov, A.M., 1954. Basic laws of turbulent mixing in the ground layer of the atmosphere. Trudy (Akademiia Nauk SSSR) Geofizicheskogo Instituta Transactions 24 (151), 163–187.

Moraes, O.L.L., Goedert, J., 1988. Kaimal's isopleths from a closure model. Boundary-Layer Meteorology 45, 83–92.

Moum, J.N., Gregg, M.C., Lien, R.-C., Carr, M.E., 1995. Comparison of turbulence kinetic energy dissipation rate estimates from two ocean microstructure profilers. Journal of Oceanic and Atmospheric Technology 12, 346–366.

Nappo, C.J., Johansson, P.-E., 1999. Summary of the Lövøanger international workshop on turbulence and diffusion in the stable planetary boundary layer. Boundary-Layer Meterology 90, 345–374.

Nieuwstadt, F.T.M., 1984. The turbulent structure of the stable, nocturnal boundary layer. Journal of the Atmospheric Sciences 41 (14), 2202–2216.

Obukhov, A.M., 1971. Turbulence in an atmosphere with a nonuniform temperature. Trudy (Akademiia Nauk SSSR) Instituta Teoreticeskoc Geofysiske. Translated and published in Boundary-Layer Meteorology 2, 7–29.

Osborn, T.R., 1980. Estimates of the local rate of vertical diffusion from dissipation measurements. Journal of the Physical Oceanography 10, 83–89.

Percival, D.B., Walden, A.T., 2000. Wavelet Methods for Time Series Analysis. Cambridge University Press, New York.

Sanford, T.B., Lien, R.-C., 1999. Turbulent properties in a homogeneous tidal bottom boundary layer. Journal of Geophysical Research 104, 1245–1257.

Sanford, T.B., Carlson, J.A., Dunlap, J.H., Prater, M.D., Lien, R.-C., 1999. An electromagnetic vorticity and velocity sensor for observing finescale kinetic fluctuations in the ocean. Journal of Atmospheric and Oceanic Technology 16, 1647–1667.

Sreenivasan, K.R., 1995. On the universality of the Kolmogorov constant. Physics of Fluids 7, 2778–2784.

Terray, E.A., Donelan, M.A., Agrawal, Y.C., Drennan, W.M., Kahma, K.K., Williams III, A.J., Hwang, P.A., Kitaigorodskii, S.A., 1996. Estimates of kinetic energy dissipation under breaking waves. Journal of Physical Oceanography 26, 792–807.

Weinstock, J., 1981. Energy dissipation rates of turbulence in the stable free atmosphere. Journal of the Atmospheric Sciences 38, 880–883.

Wyngaard, J., Kosovic, B., 1994. Similarity of structure-function parameters in the stably stratified boundary layer. Boundary-Layer Meteorology 71, 277–296.